

ENaC- and CFTR-dependent ion and fluid transport in mammary epithelia

Sasha Blaug, Kevin Hybiske, Jonathan Cohn, Gary L. Firestone, Terry E. Machen and Sheldon S. Miller

Am J Physiol Cell Physiol 281:633-648, 2001.

You might find this additional information useful...

This article cites 45 articles, 23 of which you can access free at:

<http://ajpcell.physiology.org/cgi/content/full/281/2/C633#BIBL>

This article has been cited by 3 other HighWire hosted articles:

Apical electrolyte concentration modulates barrier function and tight junction protein localization in bovine mammary epithelium

R. R. Quesnell, J. Erickson and B. D. Schultz

Am J Physiol Cell Physiol, January 1, 2007; 292 (1): C305-C318.

[Abstract] [Full Text] [PDF]

Innate immune response in CF airway epithelia: hyperinflammatory?

T. E. Machen

Am J Physiol Cell Physiol, August 1, 2006; 291 (2): C218-C230.

[Abstract] [Full Text] [PDF]

P2 purinoceptors regulate calcium-activated chloride and fluid transport in 31EG4 mammary epithelia

S. Blaug, J. Rymer, S. Jalickee and S. S. Miller

Am J Physiol Cell Physiol, April 1, 2003; 284 (4): C897-C909.

[Abstract] [Full Text] [PDF]

Medline items on this article's topics can be found at <http://highwire.stanford.edu/lists/artbytopic.dtl> on the following topics:

Biochemistry .. Membrane Conductance

Physiology .. Membrane Potential

Oncology .. Tight Junctions

Biochemistry .. Apical Membranes

Biochemistry .. Basolateral Membranes

Physiology .. Water Balance and Solute Transport

Updated information and services including high-resolution figures, can be found at:

<http://ajpcell.physiology.org/cgi/content/full/281/2/C633>

Additional material and information about *AJP - Cell Physiology* can be found at:

<http://www.the-aps.org/publications/ajpcell>

This information is current as of May 2, 2007 .

ENaC- and CFTR-dependent ion and fluid transport in mammary epithelia

SASHA BLAUG,^{1,2} KEVIN HYBISKE,¹ JONATHAN COHN,³ GARY L. FIRESTONE,¹
TERRY E. MACHEN,¹ AND SHELDON S. MILLER^{1,2}

¹Department of Molecular and Cell Biology and ²School of Optometry, University of California, Berkeley, California 94720-3200; and ³Departments of Medicine and Cell Biology, Duke University Medical Center, Durham, North Carolina 27710-0001

Received 1 March 2000; accepted in final form 26 March 2001

Blaug, Sasha, Kevin Hybiske, Jonathan Cohn, Gary L. Firestone, Terry E. Machen, and Sheldon S. Miller. ENaC- and CFTR-dependent ion and fluid transport in mammary epithelia. *Am J Physiol Cell Physiol* 281: C633–C648, 2001.—Mammary epithelial 31EG4 cells (MEC) were grown as monolayers on filters to analyze the apical membrane mechanisms that help mediate ion and fluid transport across the epithelium. RT-PCR showed the presence of cystic fibrosis transmembrane conductance regulator (CFTR) and epithelial Na⁺ channel (ENaC) message, and immunomicroscopy showed apical membrane staining for both proteins. CFTR was also localized to the apical membrane of native human mammary duct epithelium. In control conditions, mean values of transepithelial potential (apical-side negative) and resistance (R_T) are -5.9 mV and $829 \Omega \cdot \text{cm}^2$, respectively. The apical membrane potential (V_A) is -40.7 mV, and the mean ratio of apical to basolateral membrane resistance (R_A/R_B) is 2.8. Apical amiloride hyperpolarized V_A by 19.7 mV and tripled R_A/R_B . A cAMP-elevating cocktail depolarized V_A by 17.6 mV, decreased R_A/R_B by 60%, increased short-circuit current by $6 \mu\text{A}/\text{cm}^2$, decreased R_T by $155 \Omega \cdot \text{cm}^2$, and largely eliminated responses to amiloride. Whole cell patch-clamp measurements demonstrated amiloride-inhibited Na⁺ currents [linear current-voltage (I - V) relation] and forskolin-stimulated Cl⁻ currents (linear I - V relation). A capacitance probe method showed that in the control state, MEC monolayers either absorbed or secreted fluid (2 – $4 \mu\text{l} \cdot \text{cm}^{-2} \cdot \text{h}^{-1}$). Fluid secretion was stimulated either by activating CFTR (cAMP) or blocking ENaC (amiloride). These data plus equivalent circuit analysis showed that 1) fluid absorption across MEC is mediated by Na⁺ transport via apical membrane ENaC, and fluid secretion is mediated, in part, by Cl⁻ transport via apical CFTR; 2) in both cases, appropriate counterions move through tight junctions to maintain electroneutrality; and 3) interactions among CFTR, ENaC, and tight junctions allow MEC to either absorb or secrete fluid and, in situ, may help control luminal [Na⁺] and [Cl⁻].

amiloride; diphenylamine-2-carboxylate; milk secretion; patch clamp; microelectrodes; electrophysiology; cystic fibrosis; tight junctions; leaky and tight epithelia; epithelial sodium channel; cystic fibrosis transmembrane conductance regulator

THE MAMMARY GLAND is a branched, convoluted tubular organ with acinar cells that secrete macromolecules

(milk proteins, lactose, fats), salts (including Na⁺, K⁺, Ca²⁺, Cl⁻, and phosphate), and water. Human milk contains ~ 200 mM lactose, 7 mM Na⁺, 13 mM K⁺, 8 mM Ca²⁺, and 12 mM Cl⁻ and is mildly acidic (pH 6.8) (34). The initial secretion of milk by the acinar cells probably occurs as an isotonic fluid, largely driven by the production and then secretion of lactose and osmotically obliged fluid. The duct cells likely modify this fluid as it moves along the duct and passes out to the nipple. It is possible that the relatively low ionic content of milk is either generated or maintained by the reabsorptive properties of acinar and duct cells, but the specific ion channels and other transporters involved have not been described.

Abnormal fluid accumulation in the breast is common in premenopausal women (5, 6, 21, 30). As part of a project to determine how mammary cysts accumulate fluid, we began a study of the ion transport properties of the mammary epithelial cell line 31EG4. This untransformed mouse cell line appears to have properties of both acinar and ductal mammary epithelia cells (39, 42, 48). Previous experiments on primary cultures of mouse mammary epithelial cells, which are a mixture of duct and acinar cells (4), showed that Na⁺ is actively absorbed, that this absorption is stimulated by the lactogenic hormone prolactin, and that absorption is inhibited by apical amiloride, the well-known blocker of the epithelial Na⁺ channel (ENaC) (19). 31EG4 cells form polarized monolayers with tight junctions that are regulated in their “tightness” by the glucocorticoid dexamethasone, which can stop growth and induce differentiation (48). This process includes an increase in transepithelial resistance (R_T) from 100 – $300 \Omega \cdot \text{cm}^2$ to >700 – $1,000 \Omega \cdot \text{cm}^2$ and the appearance of tight junctional proteins ZO-1 and more “organized” filamentous actin. It is thought that this regulation of tight junctions recapitulates the transformation of mammary cells from a leaky to a tight epithelium characteristic of the lactating gland that must maintain a large transepithelial (blood to milk) concentration gradient for ions and macromolecules (29, 35).

The costs of publication of this article were defrayed in part by the payment of page charges. The article must therefore be hereby marked “advertisement” in accordance with 18 U.S.C. Section 1734 solely to indicate this fact.

Address for reprint requests and other correspondence: S. S. Miller, 360 Minor Hall, Univ. of California at Berkeley, Berkeley, CA 94720-2020 (E-mail: smiller@socrates.berkeley.edu).

Coincident with the increase in R_T , 31EG4 cells also express Na^+/H^+ exchange and $\text{Na}^+-\text{HCO}_3^-$ cotransport activity in the basolateral, but not the apical, membrane (41).

The goal of the present work was to determine whether the epithelial Cl^- and Na^+ channels [cystic fibrosis transmembrane conductance regulator (CFTR) and ENaC, respectively] contribute to the ion and fluid transport properties of the mammary epithelial cell line 31EG4. We reasoned that 31EG4 cells might also express CFTR and ENaC, since 1) the mammary gland and sweat glands are of similar embryological origin and have several characteristics in common, and 2) sweat duct cells express high levels of both these ion channels to allow reabsorption of salt from the fluid that flows down the duct (38). We used RT-PCR to identify the message and Western blot and immunomicroscopy to identify the proteins. In experiments utilizing transepithelial, microelectrode, and patch-clamp techniques, amiloride-inhibitable changes in voltage and resistance were used to localize ENaC to the apical membrane, and stimulation with cAMP and inhibition by diphenylamine-2-carboxylate (DPC) showed that CFTR is localized to the apical membrane. The roles of ENaC and CFTR in fluid absorption and secretion were determined by measuring amiloride- and cAMP-induced changes in fluid transport (capacitance probe method).

MATERIALS AND METHODS

Cell culture. 31EG4 cells were grown and cultured in DMEM/F-12 medium containing 5% fetal bovine serum (FBS), 5 $\mu\text{g}/\text{ml}$ insulin, and 5 $\mu\text{g}/\text{ml}$ gentamicin sulfate. Upon reaching confluency, these cells, passages 6–10, were plated onto Transwell filters (Costar) at a density of 10^5 cells/well. They were grown in DMEM/F-12 medium containing glutamine, 2% FBS, insulin, and gentamicin as described above. When the cells became confluent on the filters, 1 μM dexamethasone was added to stop growth and induce differentiation, including formation of tight junctions (48) and polarization of ion transport pathways to the apical and basolateral membranes (41). R_T and transepithelial membrane voltage potential (TEP) were estimated with an EVOM (Epithelial Voltammeter; World Precision Instruments, New Haven CT). The experiments were all carried out between 6 and 9 days after the addition of dexamethasone with no discernible differences in mean TEP or R_T .

RT-PCR. Total RNA was extracted from 31EG4 cells by using the RNazol B method (Teltest) per manufacturer's instructions. First-strand cDNA synthesis was carried out by using 0.5 μg of total RNA, 20 pM oligo(dT) primers, 0.5 mM dNTP mix, and 200 units of Moloney murine leukemia virus reverse transcriptase in a final volume of 20 μl of 50 mM Tris·HCl (pH 8.3), 75 mM KCl, and 3 mM MgCl_2 . The RNA and oligo(dT) were annealed by first mixing the two items, heating to 70°C for 2 min, and then cooling on ice, followed by the addition of the remaining reaction components. The mixture was incubated at 42°C for 1 h for first-strand synthesis and then heated to 94°C for 4 min to stop the reaction. The mixture was then diluted 1:5 with sterile distilled water. A control reaction containing no reverse transcriptase was included for each tissue-reverse transcriptase reaction to as-

sure that no genomic DNA was being amplified (data not shown).

PCR was carried out by using oligonucleotide primers (sense gtgattggagctatagcagttgtcg; antisense cccacatctggagc-cacagc) designed to cover a 463-bp region of CFTR and a 596-bp region of ENaC (sense tgcaactaccggaacttcag; antisense gtactgggtgtcattgcagg). The primers (0.5 mM final concentration) were added to a 1-ml aliquot of the first-strand synthesis mixture with the following: 0.2 mM dNTPs (each), 1.25 units of *Thermus aquaticus* polymerase, PCR buffer with Mg^{2+} (Boehringer Mannheim), and water to bring the mixture to a total volume of 50 μl . The reaction was then overlaid with two drops of mineral oil (Sigma, St. Louis, MO). The mixture was then incubated in a thermal cycler (Stratagene) with the following amplification profile: 1 cycle at 94°C for 4 min; 37 cycles at 94°C for 1 min, 55°C for 1 min, and 72°C for 1 min; and 1 cycle of 72°C for 10 min. The PCR product was run on a 1.5% agarose gel. This product was excised from the gel with a razor and then purified and sequenced by the University of California at Berkeley Sequencing Center.

Western blots. 31EG4 cells were cultured to confluence on filters as described in *Cell culture*. Proteins were isolated by placing the cells into 100 μl of protein isolation buffer containing (in mM) 65 NaCl, 2 MgCl_2 , 1 EDTA, and 5 Tris-acetate, pH 7.4, as well as the following protease inhibitors (in $\mu\text{g}/\text{ml}$): 2 aprotinin, 2 leupeptin, 1 pepstatin A, 2 antipain, 100 phenylmethylsulfonyl fluoride, 50 *N* $^\alpha$ -*p*-tosyl-*l*-lysine chloromethyl ketone, and 100 *N*-tosyl-*l*-phenylalanine chloromethyl ketone. The cells were homogenized by sonicating (Branson, Danbury, CT) on ice for 60 s. Protein concentration was determined using BCA (bicinchoninic acid) protein assay kit (Pierce, Rockford, IL). To separate protein from membranes, we incubated the sample for 4 h at room temperature (RT) in 4% digitonin (wt/vol) in 0.2 M sodium phosphate buffer, pH 8.6. Electrophoresis of the samples was carried out by using Bio-Rad Mini-Protein ready gels (7.5% Tris·HCl) and the Bio-Rad Mini-Protean cell (Hercules, CA). The running buffer contained 25 mM Tris, 200 mM glycine, and 0.1% SDS. Electroblooming of the proteins onto polyvinylidene difluoride (PVDF) membranes was carried out in a Bio-Rad Mini-Trans-Blot cell at 4°C. The transfer buffer contained 25 mM Tris and 200 mM glycine, pH 8.2–8.5. The blotted PVDF membranes were then blocked in 2% casein [in 0.1% (vol/vol) Tween 20 in PBS] for 1 h at RT and then incubated with a 1:1,000 dilution of primary anti-CFTR antibody overnight at 4°C (pAbECL1-19, peptides corresponding to amino acids 103–109, 109–114, 114–119 of CFTR; a generous gift from Genzyme). Similar procedures were used with a primary anti-ENaC antibody (β -subunit, a generous gift from Pascal Barbry). The membranes were rinsed three times (5 min each time) with Blotto (5% nonfat dried milk and 0.1% Tween 20 in PBS). The membrane was then incubated in a 1:5,000 dilution of horseradish peroxidase-conjugated anti-rabbit secondary antibody (Sigma) for 1 h at RT, followed by three rinses (5 min each time) with Blotto and then 5 min with PBS. The labeled membranes were developed by using the enhanced chemiluminescence method (NEL-10 Renaissance; NEN).

Immunohistochemistry. 31EG4 cells were grown to confluence on Transwell filters, and the monolayer and filter membranes were punched out, rinsed in PBS for 1 min at RT, and then fixed in 4% formaldehyde-PBS for 30 min. The sample was then rinsed three times, over the course of 10 min, with PBS at RT and placed in 30% sucrose-PBS solution to equilibrate overnight at 4°C. The samples were next embedded in OCT (optimum cutting temperature) compound (Tissue-Tek,

Torrance, CA) and incubated at -20°C for at least 1 h. The samples were then sectioned in 10- to 20- μm slices with a cryostat (Leica), placed on Superfrost glass slides (Fisher Scientific), and left overnight to dry at RT. Sections were rinsed for 5 min in PBS and incubated in 10% BSA-PBS solution for 2 h at RT. The slides were then incubated overnight at 4°C in 1:100 (PBS/BSA) dilutions of either polyclonal anti-CFTR or anti-ENaC (β -subunit). The sections were rinsed three times (10 min each time) in PBS at RT and then incubated in a 1:2,000 dilution of FITC-labeled secondary antibodies for 1 h at RT. The sections were finally rinsed three times (10 min each time) in PBS and mounted on coverslips with Prolong mounting solution (Molecular Probes, Eugene, OR). Images were obtained with the use of a Zeiss Axiophot microscope with a $\times 63$ objective.

Immunomicroscopy to identify CFTR in intact mammary gland was also performed on cryosections (4 μm) of promptly frozen normal human surgical specimens by using an affinity-purified rabbit antibody [a1468, a synthetic peptide corresponding to amino acids 1468–1480 of CFTR (11, 31)] at a 1:200 dilution. The specificity of a1468 as a reagent for detecting endogenously expressed CFTR in human colonocytes has been verified in a variety of tissues by immunoblot, immunoprecipitation, and immunostaining (11–13, 18, 31). Sections were incubated first with a1468 and then with a monoclonal antibody to cytokeratin 19 (ICN Biomedical, Costa Mesa, CA). Sections were then washed and incubated with TRITC- and FITC-conjugated goat F(ab')₂ fragments (Tago, Burlingame, CA). Controls for immunostaining included sections stained without primary antibody or with normal rabbit serum.

Fluid transport. Transepithelial fluid flows (J_V) were measured by using the capacitance probe technique (22, 24). A monolayer on a filter (0.5-cm² exposed area) was mounted between two water-impermeable Kel F half-chambers. J_V was determined with a very sensitive oscillator circuit (Acumasure 1000; Mechanical Technology, Albany, NY) connected to two probes, one on either side of the tissue, which measure the capacitance between the probe tips and the fluid menisci connected to each half-chamber. Ion-linked fluid is driven across the tissue from its apical to basolateral surfaces, or vice versa. Fluid movement across the epithelium is recorded by the changes in probe output voltage. Ports in the bottom of the half-chambers allow for solution and chemical composition changes on either side of the tissue. The capacitance probe in each half-chamber was calibrated by injecting 1- μl volumes of fluid and measuring the probe output in millivolts (737 mV/ μl). This technique has a resolution of ~ 1 nl/min, corresponding to a fluid transport rate approximately one-tenth the average baseline fluid transport rate seen in the present experiments. Voltage-sensing and current-passing bridges built into each half-chamber permit continuous monitoring of TEP and R_T , the latter being calculated from the voltage deflections in response to transepithelial current pulses of known magnitude. The control Ringer solution for measurements of J_V , TEP, and R_T contained (in mM) 113.5 NaCl, 5 KCl, 26 NaHCO₃, 1.8 CaCl₂, 0.8 MgSO₄, 1.0 NaH₂PO₄, and 5.5 glucose, pH 7.4. In some experiments, a cAMP cocktail was added to the control Ringer solution: 500 M 3-isobutyl-1-methylxanthine (IBMX), 100 μM 8-(4-chlorophenylthio)adenosine 3',5'-cyclic monophosphate (CPT-cAMP), and 12 μM forskolin. In other experiments, the following inhibitors were tested: 10–50 μM amiloride (to block ENaC), 0.5–1.0 mM DPC (to block CFTR), and 50 μM 5-nitro-2-(3-phenylpropylamino)benzoic acid (NPPB; to block CFTR).

Patch-clamp electrophysiology. Cells were plated on glass coverslips at low density. Patch pipettes were pulled from glass (WPI, Sarasota, FL) on a microelectrode puller (Narishige, Tokyo, Japan) and fire-polished on a microforge (Narishige) to a resistance of 2–10 M Ω when filled with intracellular solution (see below). Seal resistances were typically 10 G Ω . Data were recorded in the voltage-clamp mode with an amplifier (Axopatch-1D; Axon Instruments, Foster City, CA) connected to a personal computer with an analog-to-digital board. Voltage sweeps and currents were recorded with the use of Clampex acquisition software (Axon Instruments). Leak subtraction was not performed on any of the data. Solution changes were made via a seven-node perfusion chamber. The bath chamber was maintained at 37°C with a battery-operated resistive element mounted on the bottom of the chamber and controlled by a battery-operated feedback circuit.

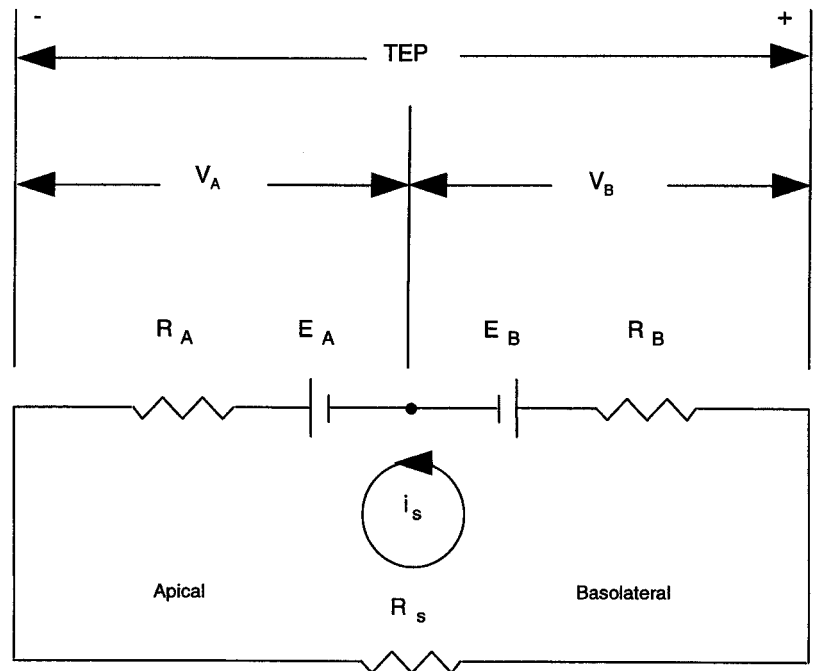
To identify CFTR, whole cell patch pipettes were filled with intracellular solution containing (in mM) 121.5 *N*-methyl-D-glucamine (NMDG)-gluconate, 13.5 NMDG-Cl, 1.8 ATP, 0.09 GTP, 9 HEPES, and 9 glucose. Extracellular solution contained (in mM) 141 NaCl, 4 KCl, 1 KH₂PO₄, 1 MgSO₄, 1 CaCl₂, 10 HEPES, and 10 glucose, with either 10 μM forskolin or 2 mM DPC added. Voltage sweeps were run from -80 mV to 100 mV, with data sampled at a frequency of 10 kHz.

Whole cell experiments were also performed in an attempt to identify ENaC in single 31EG4 cells. Cells were plated at low density and then treated with 1 μM dexamethasone for roughly 24 h before the experiment to increase cellular differentiation. Pipette solution for these experiments contained (in mM) 121.5 NMDG-gluconate, 2.7 NMDG-Cl, 0.9 CaCl₂, 0.9 MgCl₂, 9 HEPES, 4.5 glucose, 2.25 ATP, 0.09 GTP, and 9.9 EGTA. Two different extracellular solutions were employed for these experiments. Extracellular Na-gluconate solution contained (in mM) 145 Na-gluconate, 7 NaCl, 1 CaCl₂, 1 MgCl₂, 10 HEPES, and 5 glucose. Extracellular NaCl solution contained (in mM) 150 NaCl, 1 CaCl₂, 1 MgCl₂, 10 HEPES, and 5 glucose. Voltage sweeps were run from -80 mV to 100 mV, with data sampled at a frequency of 10 kHz. Conductance values were obtained by measuring the slopes of the current-voltage (*I-V*) curves at around 20 mV.

Transepithelial and microelectrode electrophysiology. The recording setup and perfusion system has been described previously (36). Transwells with confluent 31EG4 monolayers and $R_T > 300 \Omega \cdot \text{cm}^2$ were used for the electrophysiology measurements. The monolayers on filters were mounted on a nylon mesh support and clamped into a modified Ussing chamber. R_T and the ratio of the apical to basolateral membrane resistance (a) were obtained by passing 4- μA current pulses across the tissue and measuring the resultant changes in TEP and voltages across the apical (V_A) and basolateral membranes (V_B). Current pulses were bipolar, with a period of 3 s applied at various time intervals. R_T is the resulting change in TEP divided by 2 μA , and a is the ratio of voltage change in V_A divided by the change in V_B ($a = \Delta V_A / \Delta V_B$). The current-induced voltage deflections were digitally subtracted from the records for clarity. Short-circuit current (I_{sc}) measurements were performed with the use of similar chambers and electrophysiological apparatus, with TEP clamped to zero and using solution and resistance compensation. Pulses of 5 mV were often utilized to measure R_T in these experiments. The control Ringer solutions (in mM) used for measurements of TEP, R_T , and I_{sc} are identical to those used for the measurements described in *Fluid transport*.

Calculating membrane and shunt resistances and equivalent electromotive forces. The intracellular measurements were analyzed with an equivalent circuit model (see Fig. 1)

Fig. 1. Equivalent circuit for 31EG4 mammary epithelia. Apical and basolateral membranes are represented by equivalent resistance (R_A and R_B , respectively) in series with an electromotive force (E_A and E_B , respectively) that would be measured in the absence of a shunt. Shunt resistance (R_S) represents the parallel combination of the junctional complex resistance and the mechanical seal resistance around the tissue. A loop current (i_s) flows through the circuit due to the difference between the measured apical and basolateral membrane voltages (V_A and V_B , respectively). The transepithelial potential (TEP) represents the difference between V_B and V_A .



that has been previously described (26, 32). We used the microelectrode data to calculate resistances (R , in $\Omega \cdot \text{cm}^2$) and equivalent electromotive forces (E , in mV) for the apical and basolateral membranes and the shunt for 31EG4 cells. The general approach used (26) was to measure TEP as well as V_A and V_B and determine α values ($\alpha = \Delta V_A / \Delta V_B = R_A / R_B$) in control conditions and then during treatment with amiloride. This allowed us to calculate shunt resistance (R_S). It was assumed that amiloride only altered E_A and R_A . Calculation of equivalent circuit parameters was based on the following steady-state considerations

$$V_A = E_A + iR_A \quad \text{and} \quad V_B = E_B - iR_B \quad (1)$$

where i is the loop current generated by the difference in V_A and V_B , and E_A and E_B are the apical and basolateral mem-

brane potentials, respectively, that would be recorded if R_S were infinite. By definition

$$\text{TEP} = V_B - V_A \quad \text{and} \quad i = \text{TEP} / R_S \quad (2)$$

R_T is given by

$$R_T = [(R_A + R_B)R_S] / [R_A + R_B + R_S] \quad \text{and} \quad \alpha = R_A / R_B \quad (3)$$

Combining Eqs. 1 and 2 gives

$$V_A = E_A + \text{TEP}(R_A / R_S) \quad (4)$$

Similarly,

$$V_B = E_B - \text{TEP}(R_B / R_S) \quad (5)$$

Using Eq. 3 before and after (denoted with asterisk) amiloride, we obtain

$$R_S = [R_T R_T^* (\alpha^* - \alpha)] / [R_T (1 + \alpha^*) - R_T^* (1 + \alpha)] \quad (6)$$

Using Eqs. 4–6 and the data collected before and shortly after amiloride treatment, we calculated R_S and then R_A , R_B ,

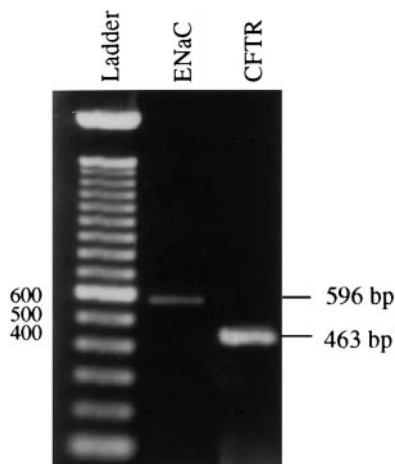


Fig. 2. PCR products for epithelial Na^+ channel (ENaC; 596 bp) and cystic fibrosis transmembrane conductance regulator (CFTR; 463 bp). The amplified products were run on a 1.5% agarose gel and stained with ethidium bromide. The 100-bp ladder is shown at left (ladder).

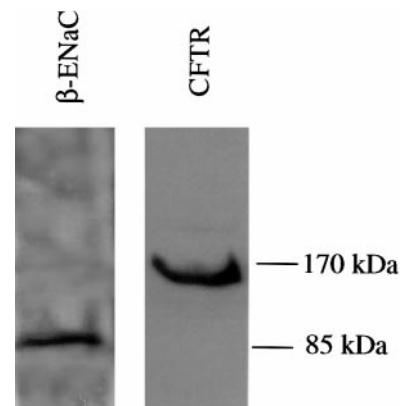


Fig. 3. Western blot analysis of CFTR and β -ENaC protein in 31EG4 cells. Cell homogenates were loaded for SDS-PAGE and analyzed subsequently by Western blotting. The migration of molecular mass markers (in kDa) is indicated. See text for details.

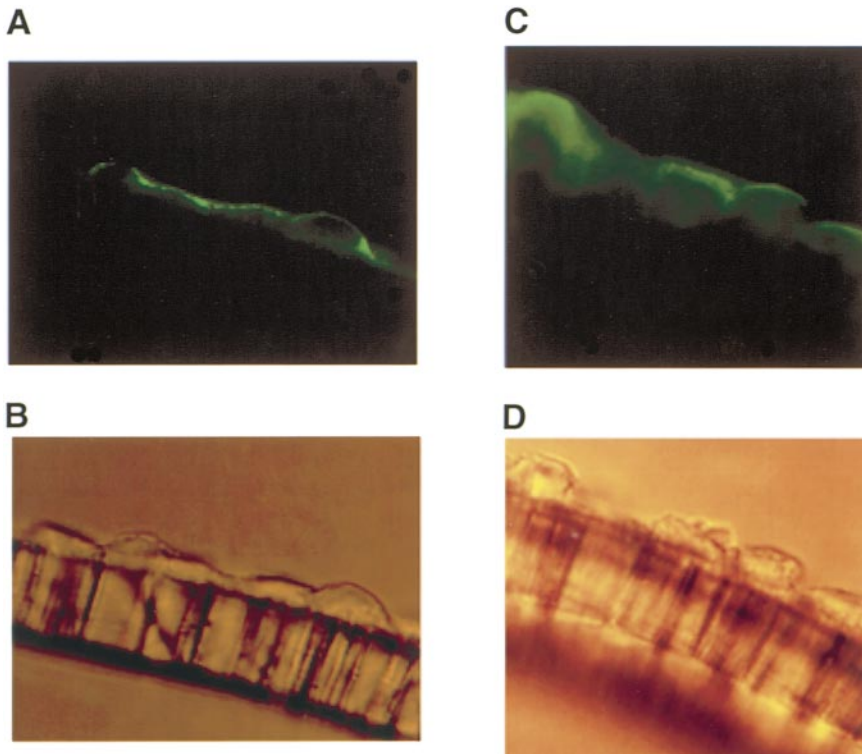
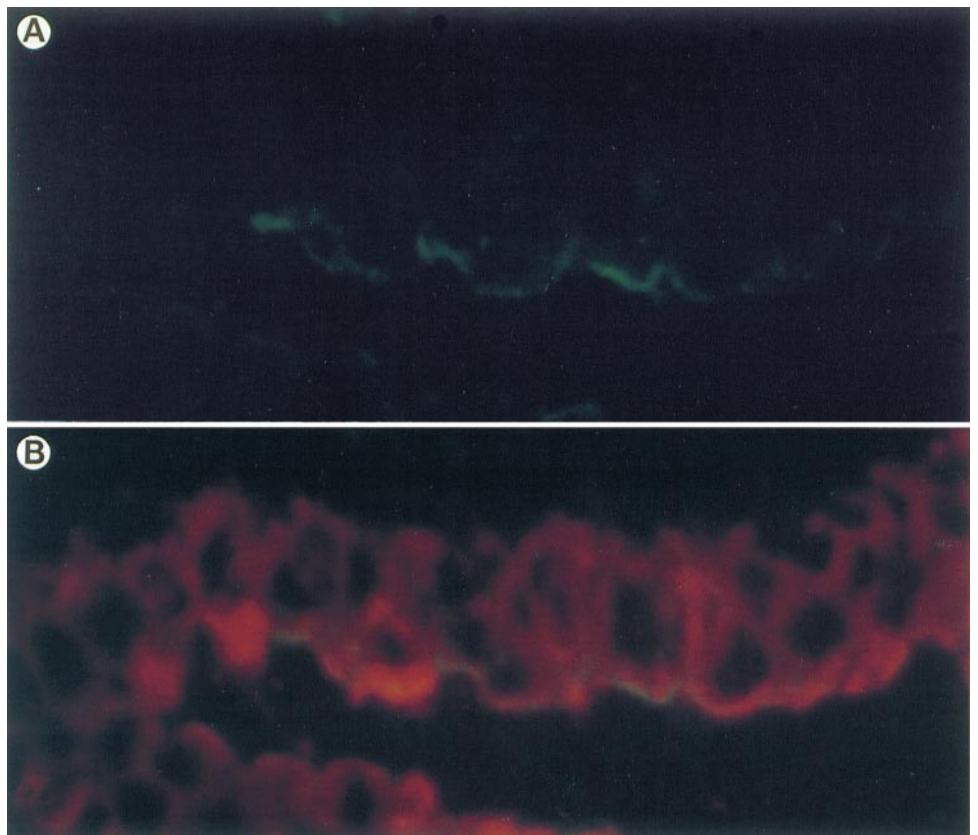


Fig. 4. Immunofluorescence localization of ENaC (A) and CFTR (C) and their respective bright-field images (B and D) in a 31EG4 monolayer. Cryostat sections were stained with primary antibodies to the β -subunit of ENaC and to CFTR and were then FITC-conjugated with secondary antibodies. The Transwell mesh is visible below the monolayer (B and D). Staining with primary antibodies showed that both ENaC (A) and CFTR (C) were located in the apical regions of the cells. Original magnifications, $\times 630$.

Fig. 5. Detection of CFTR and cytokeratin 19 in intact human breast by double-label indirect immunofluorescence with a1468 plus a monoclonal antibody to cytokeratin 19. A: a1468 staining of the apical domain of ductal epithelial cells as detected from the FITC (green) fluorescence. B: combined fluorescence with both antibodies in a double exposure showing fluorescence. TRITC fluorescence (orange-red) identifies duct cells on the basis of their content of cytokeratin 19. FITC fluorescence (green) occurs at the apical domain of these duct cells. Original magnification, $\times 400$.



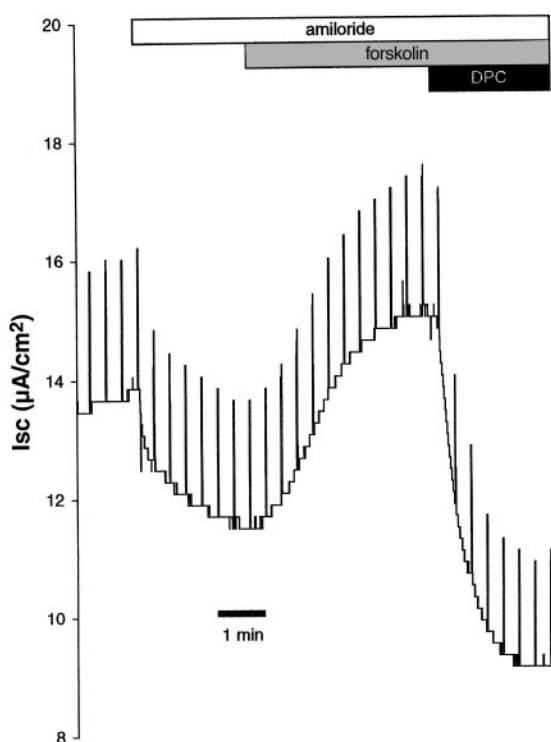


Fig. 6. Effects of amiloride, forskolin, and diphenylamine-2-carboxylate (DPC) on short-circuit current (I_{sc}) of 31EG4 monolayers. Cells grown to confluency on filters were mounted in the chamber, and I_{sc} was measured. Spikes in the I_{sc} trace represent changes induced by briefly clamping epithelium to 5 mV. Apical addition of amiloride caused I_{sc} to decrease from $\sim 13.5 \mu\text{A}/\text{cm}^2$ to $11.5 \mu\text{A}/\text{cm}^2$. Subsequent treatment with $10 \mu\text{M}$ forskolin (to increase cAMP) caused I_{sc} to increase from $13.5 \mu\text{A}/\text{cm}^2$ to $15 \mu\text{A}/\text{cm}^2$, and DPC reduced I_{sc} to $9 \mu\text{A}/\text{cm}^2$. Experiment is typical of 4 others.

E_A , and E_B for control and amiloride-treated conditions. This calculation assumes that amiloride affects only the apical membrane, while R_S and R_B remain constant.

Data are presented as means \pm SE, unless otherwise specified. Student's unpaired t -test was used to compare groups, and $P < 0.05$ is considered statistically significant.

RESULTS

PCR, Western blot analysis, and immunocytochemistry. PCR and Western blot analysis were performed on 31EG4 cells grown to confluence in the presence of dexamethasone to increase differentiation of the cells. The PCR experiments summarized in Fig. 2 showed that mRNA for both ENaC and CFTR was present in 31EG4 cells. In Fig. 3, Western blots with bands at 170 (CFTR) and 85 kDa (ENaC β subunit) indicate that both proteins were being made.

Immunomicroscopy was performed on 31EG4 cells grown to confluence on filters. As shown in Fig. 4, *A* and *B*, both ENaC and CFTR appeared to be expressed in the apical portions of the 31EG4 cells. CFTR immunoreactivity was also detected in intact human mammary glands by indirect immunofluorescence (Fig. 5). The predominant site of staining was the apical domain of the epithelial cells lining the ducts of the mammary gland. Cytokeratin staining identified duct cells and demonstrated tissue architecture for orientation.

Trans epithelial and patch-clamp electrophysiology. 31EG4 monolayers were mounted in Ussing chambers and then treated with amiloride (to block ENaC), followed by forskolin (to stimulate cAMP production and active PKA) and DPC (to block CFTR). As shown in Fig. 6, $10 \mu\text{M}$ amiloride in the apical solution decreased

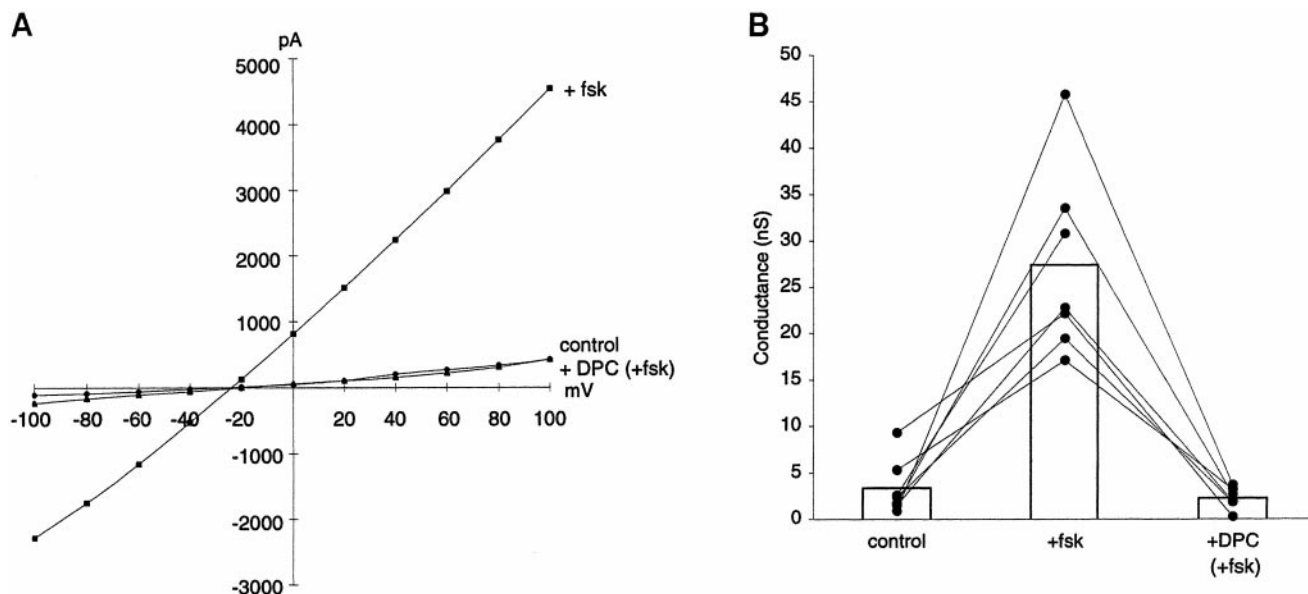


Fig. 7. Effects of forskolin and DPC on whole cell patch-clamp current, current-voltage (I - V) relationship, and conductance. *A*: whole cell I - V recording of a resting cell (control) with a basal Cl^- conductance of 1.7 nS and a reversal potential of -20 mV . Upon addition of forskolin (+fsk), conductance increased to 34 nS , and the reversal potential shifted to -25 mV . Addition of 2 mM DPC [+DPC (+fsk)] decreased the conductance to 2.7 nS and shifted reversal potential back to -20 mV . *B*: summary of 7 similar experiments. Average whole cell conductance of resting cells was $3.4 \pm 1.2 \text{ nS}$, stimulated conductance was $27.4 \pm 4.1 \text{ nS}$, and post-DPC conductance was $2.7 \pm 0.6 \text{ nS}$.

I_{sc} , although not to zero, indicating that there was some residual anion secretion or cation absorption. The identity of this ionic current has not been identified. Instead, we concentrated on determining the potential contribution of ENaC and CFTR to the ion transport properties of 31EG4 cells. In the presence of apical amiloride, forskolin (10 μ M) increased I_{sc} , and subsequent addition of apical DPC (500 μ M) decreased I_{sc} . In five experiments, amiloride decreased I_{sc} by $2.5 \pm 0.7 \mu\text{A}/\text{cm}^2$ (mean \pm SE); in the presence of amiloride, forskolin increased I_{sc} by $7.8 \pm 1.4 \mu\text{A}/\text{cm}^2$, and subsequent addition of DPC decreased I_{sc} by $5.5 \pm 0.8 \mu\text{A}/\text{cm}^2$.

Whole cell patch-clamp measurements were also performed on 31EG4 cells. As shown in Fig. 7A, forskolin increased cellular conductance from 1.7 nS to 34 nS and shifted the reversal potential from about -20 mV to -25 mV. DPC reversed the forskolin-induced changes by bringing the reversal potential and the conductance back to their resting, baseline levels. Figure 7B summarizes the effects of forskolin and DPC on 31EG4 cell conductance.

Amiloride-sensitive currents were also identified in whole cell patch-clamp experiments. These currents were quite small in the resting state (Fig. 8A), so the inhibitory effects of amiloride were difficult to identify in every cell. Figure 8A shows an experiment in which the cells were incubated in a NaCl-containing Ringer solution; the I - V curve showed small, linear currents (mean whole cell conductance = 0.6 nS, reversal potential = -15 mV). Conductance was inhibited by amiloride to 0.3 nS, and the reversal potential shifted in the negative direction to -22 mV, consistent with inhibi-

tion of ENaC. Two other experiments were also performed on cells in which the bathing solution was Na-gluconate Ringer (to eliminate contribution of Cl^- currents), and amiloride had similar effects on cell currents and conductances, although the absolute conductances were, for some unexplained reason, significantly higher. Figure 8B summarizes the results from two experiments in which the cells were incubated in a NaCl-containing Ringer and two other experiments in which the cells were bathed in Na-gluconate Ringer.

Intracellular recordings, calculated electromotive forces, and cell membrane resistances. Figure 9 shows a typical intracellular microelectrode recording with resting, unstimulated levels of V_A , V_B , TEP, R_T , and R_A/R_B . When a cocktail of forskolin, CPT-cAMP, and IBMX was added to the apical bath, there was a rapid and reversible increase in TEP, since V_A depolarized more than V_B ; concomitantly, R_T dropped and R_A/R_B decreased from 3.5 to 2. All these responses are consistent with a conductance increase of an apical membrane channel whose equilibrium potential is depolarized with respect to V_A .

As summarized in Table 1, the mean resting R_T and TEP are $829 \Omega \cdot \text{cm}^2$ and -5.9 mV, respectively. The TEP is apical-side negative, since V_B is more hyperpolarized than V_A . In addition, the mean R_A/R_B of ~ 3 indicates that the apical membrane has a threefold greater resting resistance than the basolateral membrane. Table 1 also summarizes the cAMP-induced changes in membrane voltages and resistance, which are all consistent with an increase in apical membrane conductance. From the summary data in Table 1, the calculated (Ohm's law) equivalent I_{sc} of the resting

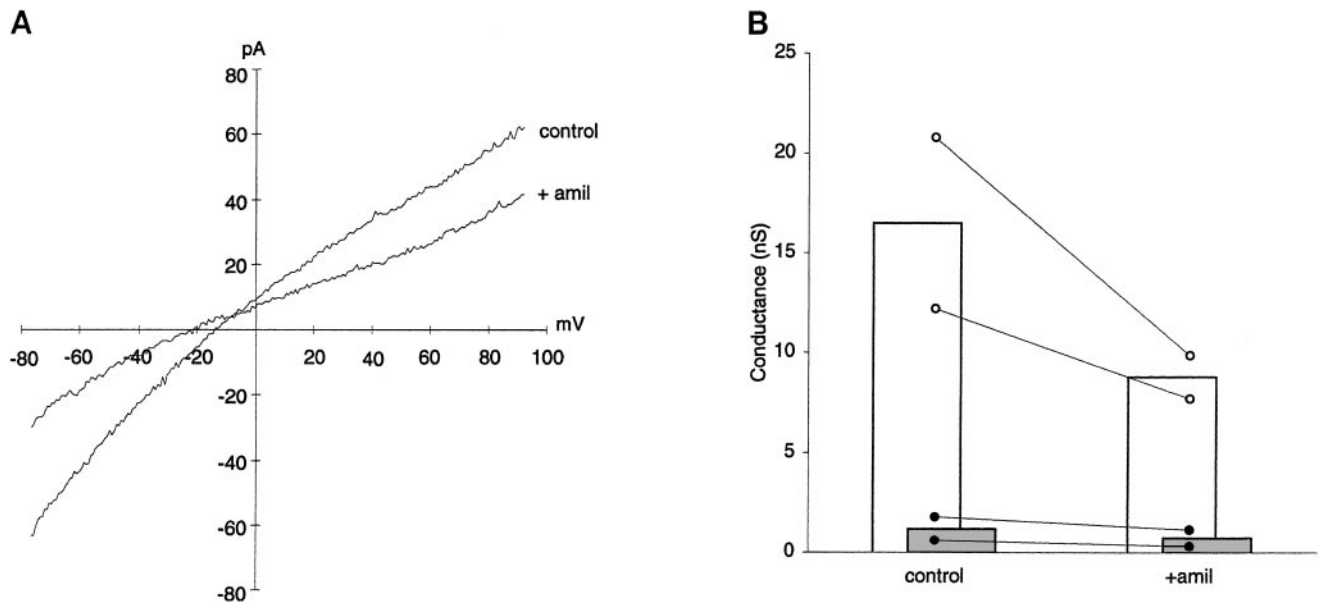


Fig. 8. Effect amiloride on whole cell patch-clamp current, I - V relationship, and conductance in NaCl and Na-gluconate Ringer solutions. A: whole cell patch recording of a resting cell (control) with a basal conductance in NaCl solution of 0.6 nS and a reversal potential of -15 mV. Addition of 10 μ M amiloride (+amil) caused conductance to decrease to 0.3 nS and shifted the reversal potential to -22 mV. B: summary of 2 experiments performed with NaCl bathing solutions (\bullet) and 2 experiments performed with Na-gluconate solutions (\circ). Average resting conductance was 1.2 nS in NaCl solution and 0.7 nS after amiloride. Average resting conductance in Na-gluconate solution was 16.5 nS, decreasing to 8.8 nS after amiloride.

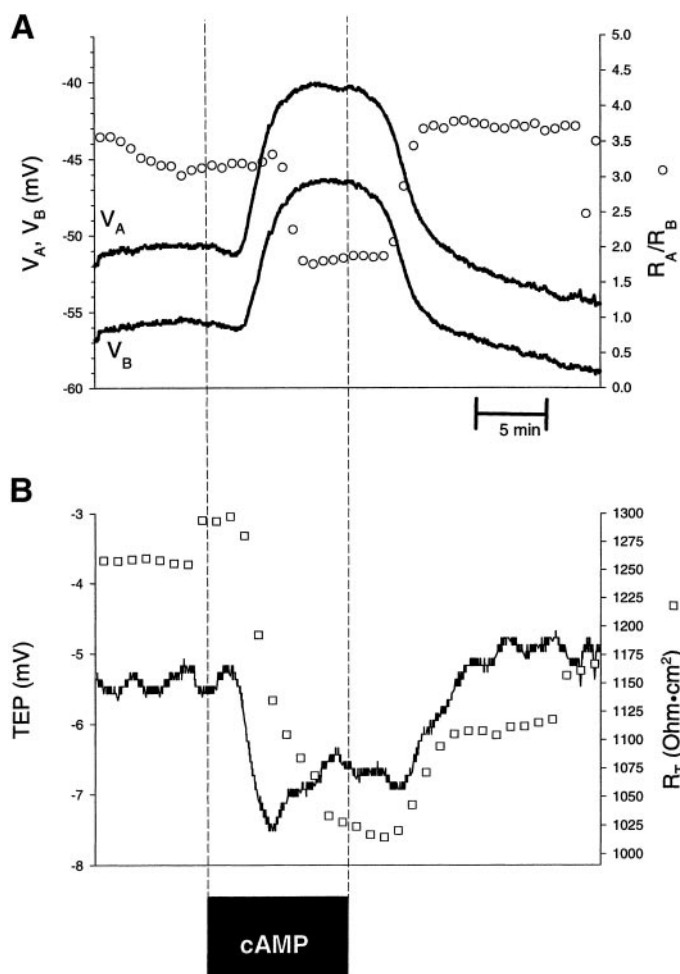


Fig. 9. Effects of cAMP cocktail on membrane voltage and resistance in 31EG4 cells. *A*: continuous traces represent V_A and V_B , and open circles represent the ratio of apical to basolateral membrane resistance (R_A/R_B). The cAMP-elevating cocktail (see MATERIALS AND METHODS) caused, after a brief delay, depolarizations of both V_A and V_B by >10 mV, whereas R_A/R_B decreased. *B*: TEP (continuous trace) increased by 2 mV, R_T (\square) decreased by $200 \Omega \cdot \text{cm}^2$, and R_A/R_B decreased by approximately a factor of 2, from 3.4 to 1.7. These results are consistent with cAMP opening Cl^- channels in the apical membrane.

monolayer increased from $7.1 \mu\text{A}/\text{cm}^2$ to $12.1 \mu\text{A}/\text{cm}^2$ after treatment with the cAMP-raising cocktail, similar to the forskolin-induced increase in I_{sc} measured in the experiment in Fig. 6. The results shown in Figs. 6

and 9 and summarized in Table 1 are consistent with the hypothesis that cAMP activates apical membrane CFTR and increases Cl^- transport from the basolateral to the apical surface at a rate of $\sim 5 \mu\text{A}/\text{cm}^2$.

Because the CFTR-blocker DPC appeared to block the forskolin-induced increases in I_{sc} (Fig. 6), it was expected that the cAMP-induced changes in cellular electrophysiology would also be blocked by NPPB, another fairly specific CFTR blocker (25, 40). In the presence of apical NPPB (see Fig. 10), the cAMP cocktail had relatively little or even opposite effects on R_T , R_A/R_B , TEP, V_A , and V_B (compare with the following control or Fig. 10). For example, the slow decrease in TEP shows that V_B depolarized faster than V_A in the presence of NPPB, opposite to what is seen for the cAMP-induced changes in TEP and membrane potential. Practically identical NPPB-induced responses were observed in four experiments. In summary, elevating cell cAMP depolarized V_A and V_B , decreased R_A/R_B and R_T , and increased TEP (Table 1). These changes and their blockade by apical NPPB (or DPC, in Fig. 6) are all consistent with the presence of CFTR at the apical membrane.

Intracellular recordings were also used to measure the effects of amiloride on membrane voltages and resistances. Results from a typical microelectrode experiment are shown in Fig. 11 where apical amiloride ($20 \mu\text{M}$) decreased TEP and increased R_T . R_A/R_B increased by more than a factor of six, and V_A hyperpolarized by 24 mV. All the electrophysiological changes were reversed when amiloride was removed from the apical bath. Similar amiloride-induced changes were obtained in 16 experiments and are summarized in Table 1. These results indicate that amiloride blocked Na^+ entry through apical ENaC.

Addition of $20 \mu\text{M}$ amiloride to the basolateral solution caused small and equal depolarizations (<5 mV) in V_A and V_B with no change in TEP, a 30% drop in R_A/R_B , and a 5% increase in R_T ($n = 3$; not shown). These small alterations in membrane voltage and resistance may have been due to the effect of amiloride on the basolateral Na^+/H^+ exchanger (41) and secondary changes in cellular pH.

The data summarized in Table 1 were used as described in MATERIALS AND METHODS to calculate resistances and electromotive forces for the apical and basolateral membranes and shunt for 31EG4 cells in

Table 1. Summary of electrophysiological data from control, cAMP-, and amiloride-treated tissues

	TEP, mV	R_T , $\Omega \cdot \text{cm}^2$	V_A , mV	V_B , mV	R_A/R_B
Untreated ($n = 32$)	-5.9 ± 0.51	828.9 ± 53.9	-40.7 ± 1.5	-46.6 ± 1.6	2.8 ± 0.23
	Δ TEP, mV	Δ R_T , $\Omega \cdot \text{cm}^2$	Δ V_A , mV	Δ V_B , mV	Δ (R_A/R_B)
Amiloride ($n = 16$)	$+3.1 \pm 0.45$	$+137.2 \pm 18.5$	-19.7 ± 1.39	-16.9 ± 1.49	$+5.8 \pm 0.49$
cAMP ($n = 20$)	-2.2 ± 0.14	-155.5 ± 14.8	$+17.6 \pm 1.0$	$+15.4 \pm 1.0$	-1.7 ± 0.18

Values are means \pm SE; n = no. of experiments. Amiloride ($20 \mu\text{M}$) and cAMP induced changes (Δ) in membrane voltage and resistance. Differences between control (untreated) and cAMP and between control and amiloride are significant in all cases ($P < 0.01$). TEP, transepithelial potential; R_T , transepithelial resistance; V_A and V_B , voltages across the apical and basolateral membranes, respectively; R_A/R_B , ratio of resistance across apical and basolateral membranes.

control and during amiloride. The results of these calculations are summarized in Table 2. The assumption (MATERIALS AND METHODS) that amiloride had no effect on R_S or R_B was tested by allowing either R_S or R_B to change up to $\pm 20\%$ after amiloride treatment. In both cases, all of the calculated parameters were within 0.5 SD of the mean values shown in Table 1, indicating that within the error of these experiments, the effects of amiloride were restricted to the apical membrane.

Comparison of amiloride effects under control and cAMP- or ATP-treated conditions. Previous experiments have shown increased Na^+ and fluid absorption in cystic fibrosis (CF) tissues (7, 20, 24), and heterologous expression of CFTR is known to decrease the activity of ENaC in both frog oocytes (27) and Madin-Darby canine kidney cells (43, 44). However, it also has been shown that ENaC activity is much reduced in freshly isolated CF sweat ducts that lack functional CFTR (38). Because 31EG4 cells express both CFTR and ENaC, we tested whether cAMP treatment could

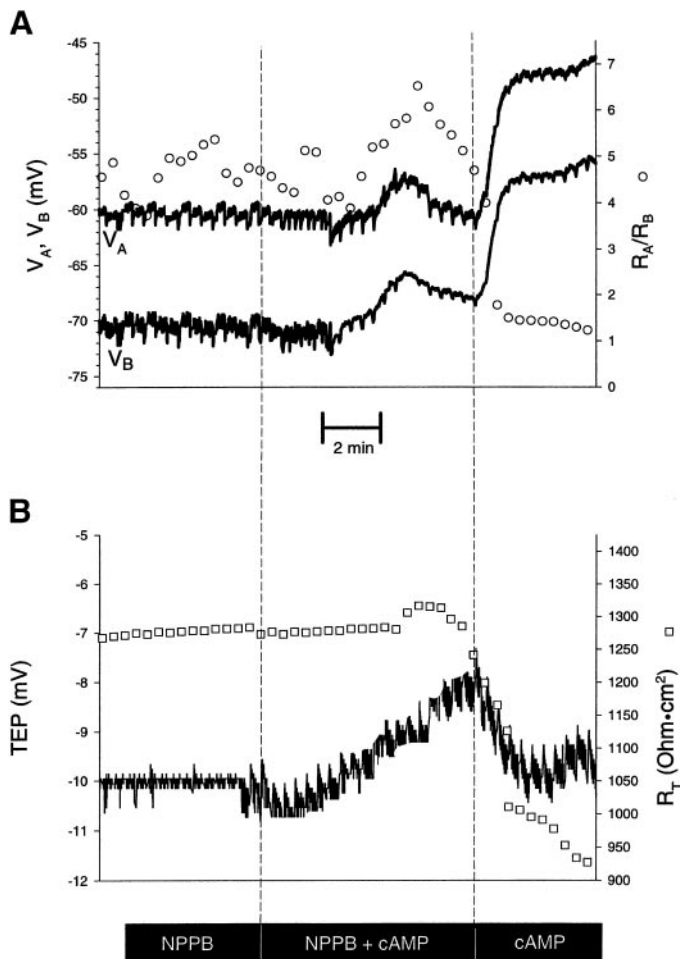


Fig. 10. cAMP-induced changes in membrane voltage and resistance are blocked by 5-nitro-2-(3-phenylpropylamino)benzoic acid (NPPB) in 31EG4 cells. **A:** continuous traces represent V_A and V_B , and open circles represent R_A/R_B . **B:** continuous trace represents TEP, and open squares represent R_T . In the presence of NPPB, the cAMP cocktail elicited only small electrophysiological responses. Removal of NPPB caused V_A and V_B to depolarize by >10 mV, whereas TEP increased and both R_T and R_A/R_B decreased.

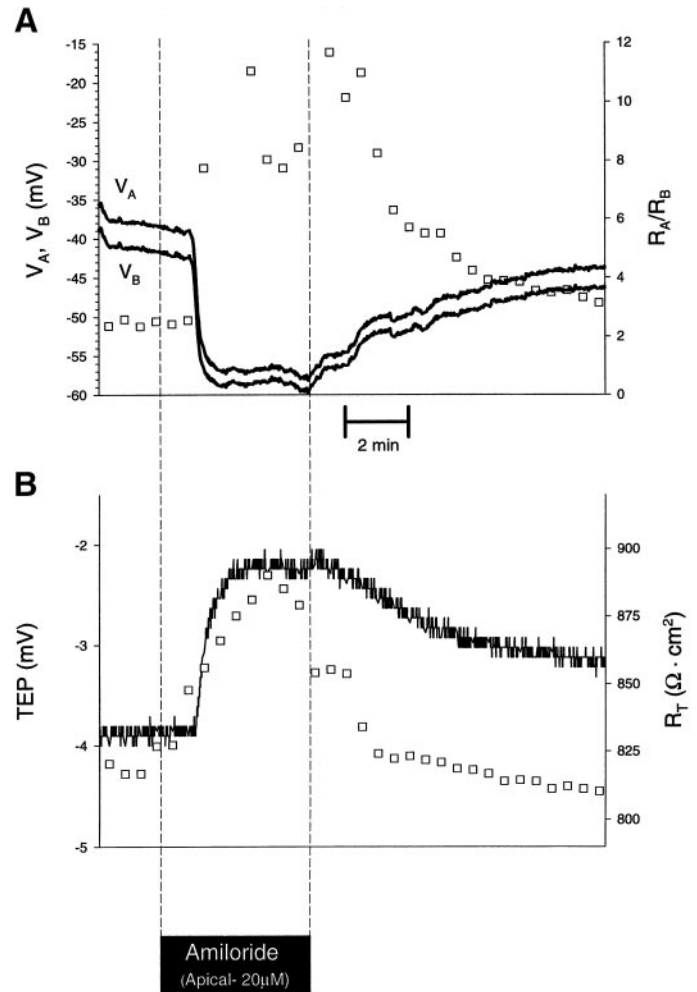


Fig. 11. Amiloride-induced changes in membrane voltage and resistance. **A:** continuous traces represent V_A and V_B , and open squares represent R_A/R_B . In control Ringer, $V_A = -46$ mV. Apical amiloride (20 μM) hyperpolarized V_A by 24 mV; R_A/R_B increased by approximately a factor of 6. **B:** TEP (continuous trace) decreased by 2 mV, and R_T (\square) increased by 100 $\Omega \cdot \text{cm}^2$. Effects of amiloride were readily reversed upon removal from the apical bath.

alter ENaC activity. A typical experiment is shown in Fig. 12A. In the first part of the experiment, amiloride (20 μM) hyperpolarized V_A by 20 mV and increased baseline R_A/R_B by a factor of 10, from 0.25 to 2.5; in addition, R_T increased and TEP decreased. Subsequent addition of the cAMP cocktail, in the continued presence of amiloride, depolarized V_A by ~ 24 mV and decreased R_A/R_B to its baseline level in control Ringer. cAMP addition also decreased R_T and increased TEP. Similar results were obtained in two other experiments (not shown). The voltage changes were somewhat larger than those exhibited in the absence of amiloride, probably because amiloride increased the driving force for Cl^- exit across the apical membrane. These results show that the blockade of ENaC activity with amiloride does not appreciably alter the cAMP-induced changes in membrane voltage and resistance.

In contrast, the data in Fig. 12B show that apical amiloride caused significantly smaller electrophysio-

Table 2. Equivalent circuit parameters calculated from control data and from electrical changes induced by addition of amiloride

	$R_A, \Omega \cdot \text{cm}^2$	$R_B, \Omega \cdot \text{cm}^2$	$R_S, \Omega \cdot \text{cm}^2$	E_A, mV	E_B, mV
Control ($n = 16$)	$1,958.9 \pm 298.2$	$776.4^* \pm 110.3$	$958.9^* \pm 93.8$	-27.9 ± 2.0	-48.4 ± 2.4
Amiloride ($n = 16$)	$6,550.2 \pm 763.6$	$776.4^* \pm 110.3$	$958.9^* \pm 93.8$	-67.9 ± 4.0	-64.3 ± 2.7

Equivalent circuit calculations are derived from summary data in Table 1. Values are means \pm SE. R_A , R_B , shunt resistance (R_S), and electromotive forces across the apical and basolateral membranes (E_A and E_B , respectively) were calculated in control and in the presence of amiloride. Asterisks signify the assumption that R_B and R_S are not altered by apical amiloride.

logical changes in the presence of cAMP stimulation: V_A and V_B hyperpolarized by only 5 mV, and R_A/R_B , R_T , and TEP hardly changed in the presence of cAMP (Table 3). Equivalent circuit calculations of membrane resistances and voltages were also performed on the subset of microelectrode experiments in which amiloride was added to monolayers that had been treated with cAMP. Results from these calculations have been summarized in Table 4. Compared with control conditions (Table 2), cAMP caused R_A to decrease from 1,958 $\Omega \cdot \text{cm}^2$ to 157 $\Omega \cdot \text{cm}^2$; in the presence of cAMP, amiloride had essentially no effect on R_A (Table 4).

The apparent reduction in ENaC activity might be secondary to cAMP-induced changes in membrane voltage or resistance. This possibility was tested by activating another set of apical Cl^- channels to see if they also reduced the effects of amiloride. We have found that the apical membrane of 31EG4 cells contains P2Y receptors that, when activated by ATP, elevate cell Ca^{2+} (Blaug and Miller, unpublished observations) and produce membrane voltage and resistance changes very similar to those produced by elevating cell cAMP: in seven experiments, apical ATP (50 μM) depolarized V_A by ~ 17 mV, from -43.9 ± 1.7 mV to -26.9 ± 1.1 mV; R_A/R_B decreased from 3.5 ± 0.2 to 1.8 ± 0.3 , and R_T decreased by 109 $\Omega \cdot \text{cm}^2$, from 518 ± 39 $\Omega \cdot \text{cm}^2$ to 409 ± 20 $\Omega \cdot \text{cm}^2$ (means \pm SE), changes not significantly different from those produced by cAMP (Table 1). If the reduction in ENaC activity were entirely dependent on cAMP-induced changes in membrane voltage or resistance, then activation of Ca^{2+} -activated Cl^- channels by ATP should also inhibit the amiloride-induced changes in TEP and R_T .

The experiment summarized in Fig. 12C tested this notion by comparing the amiloride responses in the same monolayer, first in the presence of cAMP (*top*) and then in the presence of ATP (*bottom*). Identical results were obtained independent of order. Apical amiloride characteristically decreased TEP and increased R_T , and these responses were reversible. In the presence of cAMP (which increased TEP and decreased R_T), amiloride had no significant effect on TEP or R_T . The cAMP cocktail and amiloride were removed, and the monolayer was returned to control Ringer for 30 min. Figure 12C, *bottom* (same monolayer), shows that the addition of ATP to the apical bath had effects on TEP and R_T nearly identical to those produced by cAMP. In the presence of ATP, amiloride decreased TEP and increased R_T by amounts that were very similar to those in control, untreated monolayers.

These results are summarized in Table 5. The amiloride-induced changes in TEP and R_T are significantly reduced in the presence of cAMP but not in the presence of ATP.

Fluid transport. Rates of transepithelial fluid movement along with TEP and R_T were measured under baseline, control conditions in 31EG4 monolayers grown on filters and then after the addition of either a cAMP-stimulating cocktail or amiloride to the apical bath. Figure 13 summarizes the data from a cAMP experiment. The baseline J_V was ~ 3.5 $\mu\text{l} \cdot \text{cm}^{-2} \cdot \text{h}^{-1}$, in the absorption direction. Addition of cAMP cocktail reversibly altered TEP and R_T , as in the electrophysiology experiments. Consistent with increased Cl^- secretion, cAMP reversed the direction of steady-state fluid flow from absorption to secretion (approximately -2.5 $\mu\text{l} \cdot \text{cm}^{-2} \cdot \text{h}^{-1}$); this J_V response was partially reversible.

In control Ringer, the direction and magnitude of fluid transport was variable, independent of time in culture (6–9 days).¹ Of 17 cultures (summarized in Fig. 14), 9 exhibited a baseline absorption (range: 0.5 to 7.6 $\mu\text{l} \cdot \text{cm}^{-2} \cdot \text{h}^{-1}$) and 8 exhibited a baseline secretion (range: 0.75 to -5 $\mu\text{l} \cdot \text{cm}^{-2} \cdot \text{h}^{-1}$). cAMP always caused fluid secretion,² which ranged from -1 to -8 $\mu\text{l} \cdot \text{cm}^{-2} \cdot \text{h}^{-1}$. The cAMP-induced changes in TEP and R_T were very similar for both fluid-absorbing and -secreting tissues and were very similar to the electrophysiological results summarized in Table 1. In six other monolayers, two absorbing and four secreting (Fig. 14), apical amiloride increased the mean secretory rate to -6.7 ± 4.8 $\mu\text{l} \cdot \text{cm}^{-2} \cdot \text{h}^{-1}$ (mean \pm SD).

In Fig. 15 we plotted the magnitude ($|\Delta J_V|$) of the cAMP-induced fluid-secretory response as a function of steady-state J_V . $|\Delta J_V|$ was largest for those monolayers that absorbed fluid in the baseline condition (before addition of cAMP) and lowest for those that secreted fluid. Figure 15 also shows that for monolayers in the baseline condition (no amiloride or cAMP), R_T was

¹ In a comparison of 6-, 8-, and 14-day-old cultures from the same set of cells, the mean (\pm SE) J_V was -0.9 ± 1.6 ($n = 8$; 4 absorbing), -2.6 ± 0.8 ($n = 9$; 3 absorbing), and -3.3 ± 2.9 $\mu\text{l} \cdot \text{cm}^{-2} \cdot \text{h}^{-1}$ ($n = 11$; 3 absorbing), respectively. These values are not statistically different from each other ($P > 0.3$).

² In two experiments (not shown), net fluid absorption was increased by cAMP. As expected, cAMP decreased R_T in these two experiments, but TEP also decreased, which is opposite to the results obtained in all the other experiments. This finding suggests that the electrochemical gradient for Cl^- was inward in these two cases, as was previously shown in bovine trachea (46).

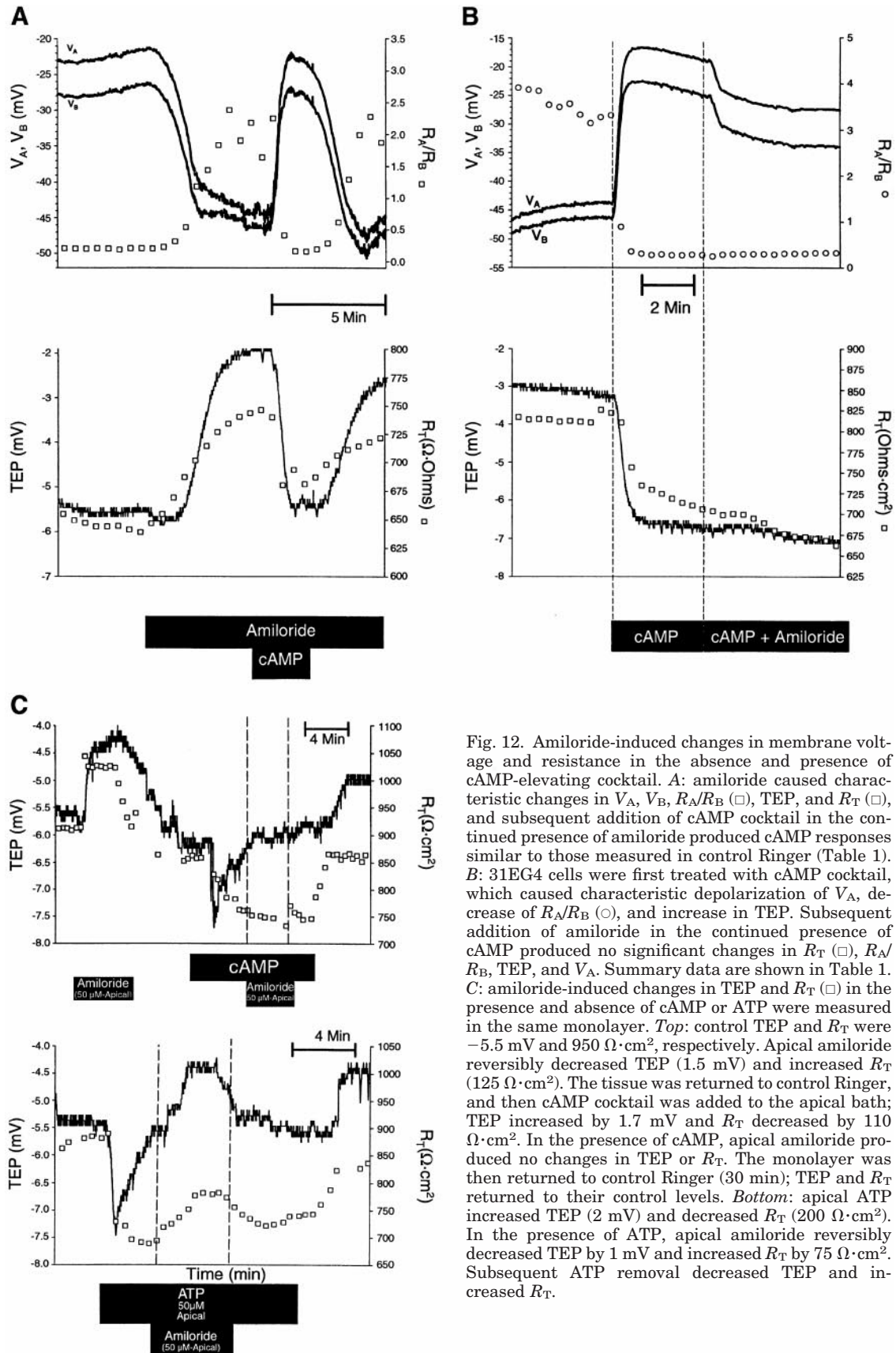


Fig. 12. Amiloride-induced changes in membrane voltage and resistance in the absence and presence of cAMP-elevating cocktail. **A**: amiloride caused characteristic changes in V_A , V_B , R_A/R_B (\square), TEP, and R_T (\square), and subsequent addition of cAMP cocktail in the continued presence of amiloride produced cAMP responses similar to those measured in control Ringer (Table 1). **B**: 31EG4 cells were first treated with cAMP cocktail, which caused characteristic depolarization of V_A , decrease of R_A/R_B (\circ), and increase in TEP. Subsequent addition of amiloride in the continued presence of cAMP produced no significant changes in R_T (\square), R_A/R_B , TEP, and V_A . Summary data are shown in Table 1. **C**: amiloride-induced changes in TEP and R_T (\square) in the presence and absence of cAMP or ATP were measured in the same monolayer. *Top*: control TEP and R_T were -5.5 mV and $950 \Omega \cdot \text{cm}^2$, respectively. Apical amiloride reversibly decreased TEP (1.5 mV) and increased R_T ($125 \Omega \cdot \text{cm}^2$). The tissue was returned to control Ringer; and then cAMP cocktail was added to the apical bath; TEP increased by 1.7 mV and R_T decreased by $110 \Omega \cdot \text{cm}^2$. In the presence of cAMP, apical amiloride produced no changes in TEP or R_T . The monolayer was then returned to control Ringer (30 min); TEP and R_T returned to their control levels. *Bottom*: apical ATP increased TEP (2 mV) and decreased R_T ($200 \Omega \cdot \text{cm}^2$). In the presence of ATP, apical amiloride reversibly decreased TEP by 1 mV and increased R_T by $75 \Omega \cdot \text{cm}^2$. Subsequent ATP removal decreased TEP and increased R_T .

Table 3. Steady-state levels of membrane voltage and resistance in the presence of cAMP alone and amiloride responses in the presence of cAMP

	TEP, mV	R_T , $\Omega \cdot \text{cm}^2$	V_A , mV	V_B , mV	R_A/R_B
cAMP ($n = 6$)	-5.9 ± 0.2	563.3 ± 86.0	-20.33 ± 2.3	-25.53 ± 2.2	0.25 ± 0.03
	ΔTEP , mV	ΔR_T , $\Omega \cdot \text{cm}^2$	ΔV_A , mV	ΔV_B , mV	$\Delta(R_A/R_B)$
cAMP + amiloride ($n = 6$)	0.0 ± 0.0	$+8.8 \pm 3.0$	-2.3 ± 0.6	-2.3 ± 0.6	$+0.03 \pm 0.005$

Values are means \pm SE. Steady-state values in cAMP + amiloride are not significantly different from those in cAMP alone (paired *t*-test).

highest in monolayers that absorbed fluid and lowest in monolayers that secreted fluid in the baseline condition.

DISCUSSION

CFTR, ENaC, ion transport, tight junctions, and mammary gland physiology. The normal (i.e., non-transformed) mammary epithelial cell line 31EG4 expresses CFTR and ENaC in the apical membranes. Messages for both CFTR and ENaC were identified, and Western blots showed that proteins with the expected molecular sizes were present. Immunomicroscopy of the cultures and intact human mammary tissue (Figs. 4 and 5) indicated that both channels are located either in or very close to the apical membrane. Although the immunomicroscopy could not determine the precise membrane locations of CFTR and ENaC, electrophysiology indicated that these channels were active in the apical membranes of the cells.

In the short-circuited condition, or when open-circuit TEP and R_T data were used to calculate equivalent I_{sc} , 31EG4 cells exhibited currents of 2–7 $\mu\text{A}/\text{cm}^2$ that were blocked by apical, but not basolateral, amiloride, consistent with the presence of functional apical ENaC. Whole cell patch-clamp measurements also demonstrated amiloride-inhibited currents and conductance as well as linear *I-V* curves expected for ENaC. Microelectrode experiments showed that amiloride hyperpolarized E_A and caused large increases in R_A , consistent with blocking apical ENaC. The comparatively smaller amiloride responses in the patch-clamp vs. the microelectrode experiments is probably due to poor seals in the patch-clamp experiments and the relatively low resistance of the shunt compared with the cellular pathway.

cAMP depolarized E_A and reduced R_A by more than a factor of 10 (compare Tables 2 and 3) and also increased basolateral-to-apical anion current (likely Cl^- or HCO_3^-) by 5 $\mu\text{A}/\text{cm}^2$; these changes were inhibited

by apical DPC or NPPB. Patch-clamp experiments also showed forskolin-stimulated, DPC-inhibitable currents and conductance as well as linear *I-V* curves. cAMP treatment also may have altered the voltage or conductance properties of other Cl^- channels at the basolateral membrane (46), but clearly a major effect of cAMP stimulation was to activate apical CFTR. 31EG4 cells also express apical membrane ATP-activated Cl^- channels and apical and basolateral K^+ channels (unpublished observations). These channels may contribute to the negative values of E_A and E_B and could also be important for ion and fluid secretion (and absorption) that occur in both baseline (control) and cAMP-stimulated conditions.

Our calculations that R_S (1,000–1,400 $\Omega \cdot \text{cm}^2$) is smaller than total cellular resistance ($R_{\text{cell}} = R_A + R_B = 2,100\text{--}2,500 \Omega \cdot \text{cm}^2$) indicate that although R_S (Table 1) is large compared with many tissues with “leaky” tight junctions ($R_S < 100\text{--}200 \Omega \cdot \text{cm}^2$; see Ref. 14), it is apparently still a major pathway for current flow. The low value of R_S compared with R_{cell} also helps keep the TEP in 31EG4 cells relatively small, -6 mV, similar to the situation in leaky epithelia (32). As discussed below, this tight junctional permeability also contributes to the ability of 31EG4 cells, a clonally derived cell line (39, 42, 48) with roughly equal distributions of ENaC and CFTR in all the cells of the monolayer (Figs. 4 and 5), to both secrete and absorb fluid (Fig. 14 and footnote 1). It will be interesting to determine whether acinar and ductal cells in situ retain this capability or if the present results represent a culture-to-culture variation in the ratio of secretory (acinar?) to absorptive (ductal?) epithelial cells.

The present demonstration of functional ENaC in the apical membrane of 31EG4 cells is consistent with previous experiments showing amiloride-sensitive Na^+ absorption across short-circuited primary cultures of both midpregnant and lactating mammary gland cells (3). Similarly, localization of CFTR to the luminal

Table 4. Equivalent circuit parameters calculated from changes induced by cAMP in the absence and presence of amiloride

	R_A , $\Omega \cdot \text{cm}^2$	R_B , $\Omega \cdot \text{cm}^2$	R_S , $\Omega \cdot \text{cm}^2$	E_A , mV	E_B , mV
cAMP ($n = 6$)	157.4 ± 26.4	$760.2^* \pm 139.8$	$1,848.6^* \pm 426.6$	-19.7 ± 2.4	-28.8 ± 1.6
cAMP + amiloride ($n = 6$)	178.8 ± 26.4	$760.2^* \pm 139.8$	$1,848.6^* \pm 426.6$	-22.0 ± 2.7	-31.11 ± 1.8

Equivalent circuit calculations are derived from summary data in Table 3. Values are means \pm SE. The cAMP-induced changes in apical membrane resistance and electromotive force are compared in the absence and presence of amiloride. Asterisks signify the assumption that R_B and R_S are not altered by apical amiloride.

Table 5. Comparison of effects of cAMP, ATP, and amiloride on TEP and R_T

	TEP, mV	R_T , $\Omega \cdot \text{cm}^2$
Control ($n = 12$)	-4.44 ± 0.49	674.7 ± 51.6
	ΔTEP , mV	ΔR_T , $\Omega \cdot \text{cm}^2$
ATP ($n = 7$)	-2.0 ± 0.36	-121 ± 14.8
cAMP ($n = 6$)	-1.9 ± 0.34	-110 ± 9.4
Control + amiloride ($n = 12$)	$+0.99 \pm 0.08$	$+90.5 \pm 8.6$
ATP + amiloride ($n = 7$)	$+0.69 \pm 0.04$	$+69.8 \pm 10.7$
cAMP + amiloride ($n = 6$)	$+0.03 \pm 0.02$	$+7.7 \pm 1.7$

Values are means \pm SE. Control values were measured in 31EG4 monolayers. ATP- and cAMP-induced changes in TEP and R_T are statistically indistinguishable from control values. Amiloride-induced changes were then measured in the absence or presence of ATP or cAMP. Amiloride-induced changes in TEP and R_T in the presence of cAMP were significantly reduced compared with those observed in control or in the presence of ATP ($P < 0.001$).

membrane of 31EG4 cells is consistent with the presence of apical CFTR in native human mammary duct cells (Fig. 5). Our results therefore indicate that ENaC and CFTR of mammary duct cells may be involved in generating or maintaining the characteristic Na^+ and Cl^- concentrations of milk (34).

ENaC and CFTR also may be involved in the abnormal generation and accumulation of breast fluid (so-called cystic disease of the breast) that occurs in 7–10% of women in Western countries, mainly in the premenopausal decade. There is now strong evidence to indicate that these women are at a two- to fourfold higher risk of later developing breast cancer (5, 8, 10, 16, 30). Although the chemical compositions of these fluid-filled cysts are quite complicated (1, 9), there appears to be a distinct pattern of Na^+ and Cl^- concentrations (17, 33) that could reflect alterations in luminal CFTR and ENaC activity. Clinically, it has been shown that tamoxifen reduces the number and size of such cysts (28). Because tamoxifen can block Cl^- channels (15, 47), it may be exerting its therapeutic effect by decreasing fluid secretion.

Effects of cAMP on CFTR and ENaC: evidence for cross talk? cAMP caused, in addition to the expected increase in CFTR activity and consequent drop in R_T and R_A , an almost complete inhibition of the amiloride-induced changes in TEP, R_T , R_A/R_B , and R_A (Fig. 12B; Tables 1–4). This apparent inhibitory effect of activated CFTR on ENaC may be understood by a direct interaction between the channels or indirectly by other mechanisms. 1) The amiloride-induced voltage re-

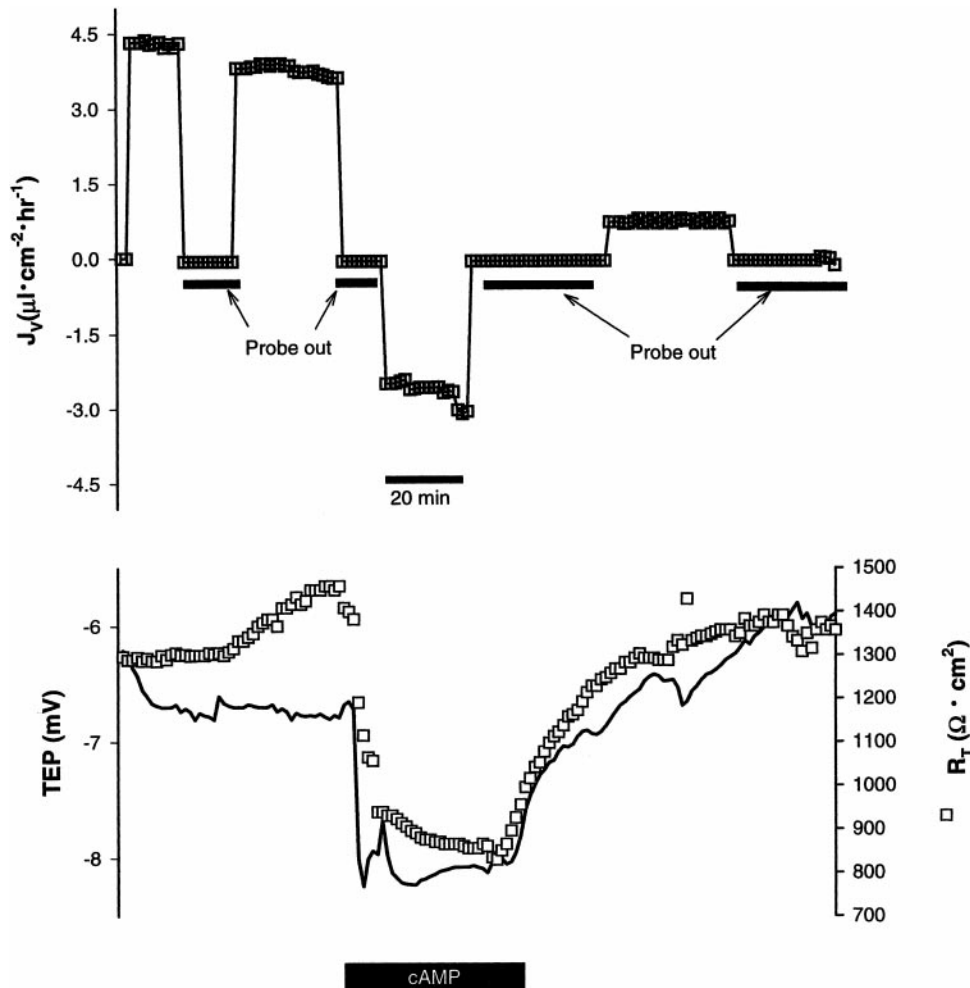


Fig. 13. cAMP-induced stimulation of steady-state fluid secretion. Apical addition of the cAMP cocktail reversed the direction of net steady-state fluid transport from absorption ($3.5 \mu\text{l} \cdot \text{cm}^{-2} \cdot \text{h}^{-1}$) to secretion ($-3.0 \mu\text{l} \cdot \text{cm}^{-2} \cdot \text{h}^{-1}$) and simultaneously increased TEP and decreased R_T consistent with the electrophysiological responses summarized in Table 1. The obligatory control-to-control solution change (probes out; see MATERIALS AND METHODS) during the first 40 min produced very little change in J_V , TEP, and R_T (\square). Removal of cAMP from the apical bath brought J_V back to absorption at $\sim 1.0 \mu\text{l} \cdot \text{cm}^{-2} \cdot \text{h}^{-1}$. The electrical changes were also reversible.

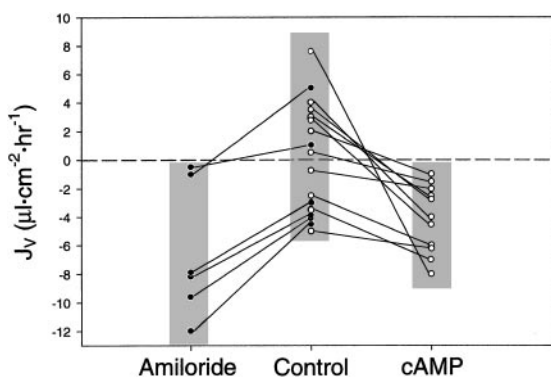


Fig. 14. Summary of fluid transport experiments with cAMP ($n = 11$) or amiloride ($n = 6$) addition. A subset of monolayers ($n = 9$) absorbed fluid at a mean J_V of $3.6 \pm 1.1 \mu\text{l}\cdot\text{cm}^{-2}\cdot\text{h}^{-1}$. Another subset of cultures ($n = 8$) secreted fluid at a mean rate of $-4.6 \pm 0.8 \mu\text{l}\cdot\text{cm}^{-2}\cdot\text{h}^{-1}$. Both cAMP and amiloride induced fluid secretion.

sponses may have been decreased because cAMP depolarized the apical membrane and reduced the driving force for Na^+ entry. However, similar inhibitory effects were seen in other experiments (not shown) in which the apical membrane was current-clamped close to its resting level in the absence of cAMP. 2) The cAMP-induced increase in apical membrane conductance may have been sufficiently large to mask the amiloride-induced changes in membrane resistance and voltage. Against that possibility are the data summarized in Fig. 12 and Table 5, which show that cAMP and ATP had practically identical effects on TEP and R_T (and V_A and R_A/R_B ; not shown) but that the amiloride responses were totally obliterated in cAMP and relatively unaffected by ATP. However, the conclusion that activation of CFTR inhibits ENaC is not certain (27, 43) because the cAMP-induced, but not the ATP-induced, increase in apical membrane conductance may have been sufficient to mask the amiloride-induced changes in membrane resistance and voltage. A more definitive experiment would be to measure the amiloride-induced changes in R_A/R_B in ATP- vs. cAMP-treated cells. However, we have been unable to hold microelectrode penetrations long enough to make this comparison.

Critical role of tight junctions in ion and fluid transport. The present data based on 31EG4 monolayers and evidence from other epithelial systems (25, 37) indicate that net vectorial transport depends critically on ENaC and CFTR operating in concert with the tight junctions. Fluid absorption is mainly controlled by the transport of Na^+ down its electrochemical gradient through apical ENaC, while fluid secretion is regulated by cell-to-lumen movement of Cl^- and/or HCO_3^- through cAMP-stimulated CFTR. In both cases, the obligatory movement of counterions (cations to accompany active Cl^- secretion and anions to accompany active Na^+ absorption) likely takes place predominantly through leaky tight junctions driven by the basal side-positive TEP. Thus "leaky" tight junctions are important for the ability of an epithelium to exhibit both absorption and secretion.

The net balance between secretion and absorption in 31EG4 cells may be determined in part by the activity of CFTR in the apical membrane. This idea is consistent with the observation that fluid absorption increases monotonically with R_T , and the cAMP-induced alteration in J_V is smallest for control tissues that absorbed fluid (Fig. 15). Thus, when CFTR conductance is lowest, R_T is highest, and the monolayers absorb Na^+ , Cl^- , and fluid. Subsequent elevation of cell cAMP could then activate the maximum number of CFTR channels and produce the maximum alteration in J_V (Fig. 15). Conversely, cultures that have a relatively low R_T may have a relatively large complement of active CFTR in the apical membrane and therefore secrete fluid in the basal state (Fig. 15); secretion is increased by amiloride block of ENaC (Fig. 14).

The tight junctions will also play a role in determining secretion vs. absorption because the intraepithelial current ($i = \text{TEP}/R_S$) (32), determined in part by the low resistance of the junctions ($R_S < R_A + R_B$), hyperpolarizes V_A , thereby increasing Na^+ entry (ENaC) into and Cl^- (CFTR) exit from the cells. During cAMP stimulation V_A depolarizes by 18 mV (Table 1), and the increase in fluid secretion indicates that the net electrochemical gradient for Cl^- is outward across the apical membrane.

These considerations emphasize the importance of the integrated activities of ion channels, tight junctions, and ion transporters in determining the direction of net Cl^- movement through CFTR. They also suggest a functional distinction among epithelia with apical ENaC and CFTR. Epithelia with tight junctions that are essentially impermeable to ions can only absorb salts and fluid via the cellular pathway. In these

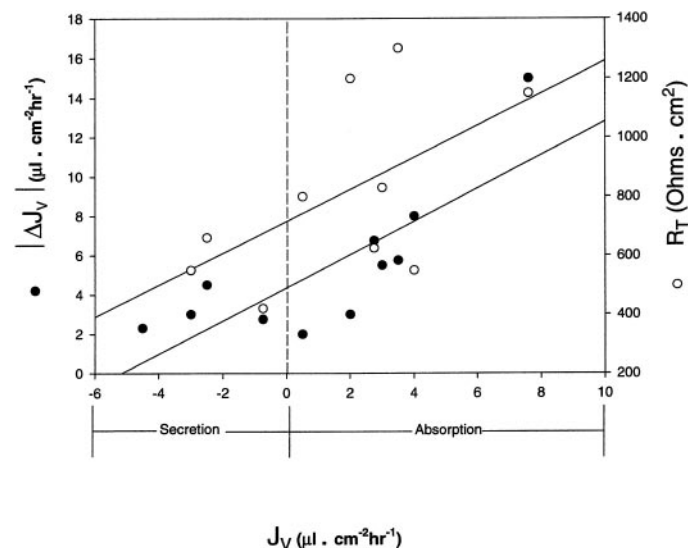


Fig. 15. Magnitude of cAMP-induced fluid secretory response ($|\Delta J_V|$) and R_T are plotted as a function of baseline, steady-state J_V in 31EG4 cells. cAMP-induced fluid secretion rate and R_T increase linearly (as net fluid absorption rate increases). The correlation coefficients, 0.6 and 0.8, respectively, are statistically significant ($P < 0.01$).

tissues, the shunt current is zero, and V_A is sufficiently depolarized such that the electrochemical driving forces for both Cl^- and Na^+ are inward across the apical membrane. Therefore, activation of CFTR with cAMP elicits absorption of Cl^- , Na^+ , and fluid through the cells (see footnote 2 in *Fluid transport*). Examples include human sweat ducts and bovine trachea (38, 46) and also may be true in the lactating mammary gland, which has large lumen-negative TEP (-35 mV), characteristic of all tight epithelia, and low concentrations of Na^+ and Cl^- in the milk (35).

In contrast, epithelia like 31EG4 cells that have relatively leaky junctions generate a shunt current that hyperpolarizes V_A , increasing Cl^- exit (CFTR) and Na^+ entry (ENaC) across the apical membrane. The conductance of the shunt to anions and cations and the existence of a TEP permit these cells to either secrete or absorb salts and fluid, depending on the ratio of ENaC to CFTR conductance and on the direction and magnitude of the electrochemical driving forces for these ions across the apical membrane. This also appears to be the case in airway submucosal glands. When CFTR is activated, these cells secrete fluid driven by the transport of HCO_3^- and Cl^- through CFTR (2, 23, 45) with Na^+ following through ion-permeable tight junctions to maintain electroneutrality. In CF, when CFTR is inactive, submucosal gland cells absorb Na^+ (through ENaC), Cl^- (through the paracellular pathway), and fluid (25). This capability to both secrete and absorb fluids also may be characteristic of the nonlactating mammary gland (with its leaky tight junctions) (35).

We thank Connie Yu for help with experiments summarized in Fig. 6 and Van Nguyen, Steve Jalickee, and Natalia Zhuravel for experiments summarized in Fig. 14. We also thank Beate Illek, Horst Fischer, and Jonathan Widdicombe for helpful comments on an earlier version of the manuscript.

This work was supported by grants from the Department of the Army Breast Cancer Research Program DAMD17-96-1-6315 (S. S. Miller), DAMD17-97-5231 (T. E. Machen), California Breast Cancer Research Program 5JB-0077 (S. S. Miller), and National Institute of Diabetes and Digestive and Kidney Diseases Grant DK-51799 (T. E. Machen).

REFERENCES

1. **Angeli A, Dogliotti L, Naldoni C, Orlandi F, Puligheddu B, Caraci P, Bucchi L, Torta M, and Bruzzi P.** Steroid biochemistry and categorization of breast cyst fluid: relation to breast cancer risk. *J Steroid Biochem Mol Biol* 49: 333–339, 1994.
2. **Ballard ST, Trout L, Bebok Z, Sorscher EJ, and Crews A.** CFTR involvement in chloride, bicarbonate, and liquid secretion by airway submucosal glands. *Am J Physiol Lung Cell Mol Physiol* 277: L694–L699, 1999.
3. **Bisbee CA.** Alterations in electrophysiology of cultured BALB/cfC3H mouse mammary epithelium associated with neoplastic transformation. *Cancer Lett* 14: 237–242, 1981.
4. **Bisbee CA, Machen TE, and Bern HA.** Mouse mammary epithelial cells on floating collagen gels: transepithelial ion transport and effects of prolactin. *Proc Natl Acad Sci USA* 76: 536–540, 1979.
5. **Bodian CA.** Benign breast diseases, carcinoma in situ, and breast cancer risk. *Epidemiol Rev* 15: 177–187, 1993.
6. **Bodian CA, Lattes R, and Perzin KH.** The epidemiology of gross cystic disease of the breast confirmed by biopsy or by aspiration of cyst fluid. *Cancer Detect Prev* 16: 7–15, 1992.
7. **Boucher RC.** Human airway ion transport. Part one. *Am J Respir Crit Care Med* 150: 271–281, 1994.
8. **Bundred NJ, West RR, Dowd JO, Mansel RE, and Hughes LE.** Is there an increased risk of breast cancer in women who have had a breast cyst aspirated? *Br J Cancer* 64: 953–955, 1991.
9. **Caputo E, Manco G, Mandrich L, and Guardiola J.** A novel aspartyl proteinase from apocrine epithelia and breast tumors. *J Biol Chem* 275: 7935–7941, 2000.
10. **Ciatto S, Biggeri A, Rosselli Del Turco M, Bartoli D, and Iossa A.** Risk of breast cancer subsequent to proven gross cystic disease. *Eur J Cancer* 26: 555–557, 1990.
11. **Cohn JA, Melhus O, Page LJ, Dittrich KL, and Vigna SR.** CFTR: development of high-affinity antibodies and localization in sweat gland. *Biochem Biophys Res Commun* 181: 36–43, 1991.
12. **Cohn JA, Nairn AC, Marino CR, Melhus O, and Kole J.** Characterization of the cystic fibrosis transmembrane conductance regulator in a colonocyte cell line. *Proc Natl Acad Sci USA* 89: 2340–2344, 1992.
13. **Cohn JA, Strong TV, Picciotto MR, Nairn AC, Collins FS, and Fitz JG.** Localization of the cystic fibrosis transmembrane conductance regulator in human bile duct epithelial cells. *Gastroenterology* 105: 1857–1864, 1993.
14. **Diamond JM.** Channels in epithelial cell membranes and junctions. *Fed Proc* 37: 2639–2643, 1978.
15. **Dick GM, Kong ID, and Sanders KM.** Effects of anion channel antagonists in canine colonic myocytes: comparative pharmacology of Cl^- , Ca^{2+} and K^+ currents. *Br J Pharmacol* 127: 1819–1831, 1999.
16. **Dixon JM, McDonald C, Elton RA, and Miller WR.** Risk of breast cancer in women with palpable breast cysts: a prospective study. Edinburgh Breast Group. *Lancet* 353: 1742–1745, 1999.
17. **Dogliotti L, Orlandi F, Caraci P, Puligheddu B, Torta M, and Angeli A.** Biochemistry of breast cyst fluid. An approach to understanding intercellular communication in the terminal duct lobular units. *Ann NY Acad Sci* 586: 17–28, 1990.
18. **Engelhardt JF, Yankaskas JR, Ernst SA, Yang Y, Marino CR, Boucher RC, Cohn JA, and Wilson JM.** Submucosal glands are the predominant site of CFTR expression in the human bronchus. *Nat Genet* 2: 240–248, 1992.
19. **Firsov D, Robert-Nicoud M, Gruender S, Schild L, and Rossier BC.** Mutational analysis of cysteine-rich domains of the epithelium sodium channel (ENaC). Identification of cysteines essential for channel expression at the cell surface. *J Biol Chem* 274: 2743–2749, 1999.
20. **Grubb BR and Boucher RC.** Enhanced colonic Na^+ absorption in cystic fibrosis mice versus normal mice. *Am J Physiol Gastrointest Liver Physiol* 272: G393–G400, 1997.
21. **Haagensen CD.** The relationship of gross cystic disease of the breast and carcinoma. *Ann Surg* 185: 375–376, 1977.
22. **Hughes BA, Miller SS, and Machen TE.** Effects of cyclic AMP on fluid absorption and ion transport across frog retinal pigment epithelium. Measurements in the open-circuit state. *J Gen Physiol* 83: 875–899, 1984.
23. **Inglis SK, Corboz MR, Taylor AE, and Ballard ST.** Effect of anion transport inhibition on mucus secretion by airway submucosal glands. *Am J Physiol Lung Cell Mol Physiol* 272: L372–L377, 1997.
24. **Jiang C, Finkbeiner WE, Widdicombe JH, McCray PB Jr, and Miller SS.** Altered fluid transport across airway epithelium in cystic fibrosis. *Science* 262: 424–427, 1993.
25. **Jiang C, Finkbeiner WE, Widdicombe JH, and Miller SS.** Fluid transport across cultures of human tracheal glands is altered in cystic fibrosis. *J Physiol (Lond)* 501: 637–647, 1997.
26. **Joseph DP and Miller SS.** Apical and basal membrane ion transport mechanisms in bovine retinal pigment epithelium. *J Physiol (Lond)* 435: 439–63, 1991.
27. **Kunzelmann K, Kiser GL, Schreiber R, and Riordan JR.** Inhibition of epithelial Na^+ currents by intracellular domains of the cystic fibrosis transmembrane conductance regulator. *FEBS Lett* 400: 341–344, 1997.

28. **Leis HP Jr.** The role of tamoxifen in the prevention and treatment of benign and malignant breast lesions: a chemopreventive. *Int Surg* 78: 176–182, 1993.
29. **Linzell J, Peaker M, and Taylor J.** The effects of prolactin and oxytocin on milk secretion and on the permeability of the mammary epithelium in the rabbit. *J Physiol (Lond)* 253: 547–563, 1975.
30. **Malatesta M, Mannello F, Sebastiani M, Cardinali A, Marcheggiani F, Reno F, and Gazzanelli G.** Ultrastructural characterization and biochemical profile of human gross cystic breast disease. *Breast Cancer Res Treat* 48: 211–219, 1998.
31. **Marino CR, Matovcik LM, Gorelick FS, and Cohn JA.** Localization of the cystic fibrosis transmembrane conductance regulator in pancreas. *J Clin Invest* 88: 712–716, 1991.
32. **Miller SS and Steinberg RH.** Passive ionic properties of frog retinal pigment epithelium. *J Membr Biol* 36: 337–372, 1977.
33. **Molina R, Filella X, Herranz M, Prats M, Velasco A, Zanon G, Martinez-Osaba MJ, and Ballesta AM.** Biochemistry of cyst fluid in fibrocystic disease of the breast. Approach to classification and understanding of the mechanism of formation. *Ann NY Acad Sci* 586: 29–42, 1990.
34. **Neville MC.** The physiological basis of milk secretion. *Ann NY Acad Sci* 586: 1–11, 1990.
35. **Nguyen DA and Neville MC.** Tight junction regulation in the mammary gland. *J Mammary Gland Biol Neoplasia* 3: 233–246, 1998.
36. **Peterson W, Meggyesy C, Yu K, and Miller SS.** Extracellular ATP activates calcium signaling, ion and fluid transport in retinal pigment epithelium. *J Neurosci* 17: 2324–2337, 1997.
37. **Peterson WM, Quong JN, and Miller SS.** Mechanisms of fluid transport in retinal pigment epithelium. In: *The Third Great Basin Visual Science Symposium on Retinal Research*, 1998, vol. III, p. 34–42.
38. **Reddy MM, Light MJ, and Quinton PM.** Activation of the epithelial Na⁺ channel (ENaC) requires CFTR Cl⁻ channel function. *Nature* 402: 301–304, 1999.
39. **Reichmann E, Ball R, Groner B, and Friis RR.** New mammary epithelial and fibroblastic cell clones in coculture form structures competent to differentiate functionally. *J Cell Biol* 108: 1127–1138, 1989.
40. **Schultz BD, Singh AK, Devor DC, and Bridges RJ.** Pharmacology of CFTR chloride channel activity. *Physiol Rev* 79, Suppl: 109–144, 1999.
41. **Sjaastad MD, Zettl KS, Parry G, Firestone GL, and Machen TE.** Hormonal regulation of the polarized function and distribution of Na/H exchange and Na/HCO₃ cotransport in cultured mammary epithelial cells. *J Cell Biol* 122: 589–600, 1993.
42. **Strange R, Li F, Friis RR, Reichmann E, Haenni B, and Burri PH.** Mammary epithelial differentiation in vitro: minimum requirements for a functional response to hormonal stimulation. *Cell Growth Differ* 2: 549–559, 1991.
43. **Stutts MJ, Canessa CM, Olsen JC, Hamrick M, Cohn JA, Rossier BC, and Boucher RC.** CFTR as a cAMP-dependent regulator of sodium channels. *Science* 269: 847–850, 1995.
44. **Stutts MJ, Rossier BC, and Boucher RC.** Cystic fibrosis transmembrane conductance regulator inverts protein kinase A-mediated regulation of epithelial sodium channel single channel kinetics. *J Biol Chem* 272: 14037–14040, 1997.
45. **Trout L, King M, Feng W, Inglis SK, and Ballard ST.** Inhibition of airway liquid secretion and its effect on the physical properties of airway mucus. *Am J Physiol Lung Cell Mol Physiol* 274: L258–L263, 1998.
46. **Uyekubo SN, Fischer H, Maminishkis A, Illek B, Miller SS, and Widdicombe JH.** cAMP-dependent absorption of chloride across airway epithelium. *Am J Physiol Lung Cell Mol Physiol* 275: L1219–L1227, 1998.
47. **Von Weikersthal SF, Barrand MA, and Hladky SB.** Functional and molecular characterization of a volume-sensitive chloride current in rat brain endothelial cells. *J Physiol (Lond)* 516: 75–84, 1999.
48. **Zettl KS, Sjaastad MD, Riskin PM, Parry G, Machen TE, and Firestone GL.** Glucocorticoid-induced formation of tight junctions in mouse mammary epithelial cells in vitro. *Proc Natl Acad Sci USA* 89: 9069–9073, 1992.